The eigenvalues can now take on imaginary values, however the functions ϕ_m still comprise a complete orthogonal set.[3] Although Eq. (A1) is apparently a solution to Eq. (3), it has two distinct disadvantages. It diverges slowly and, because its derivative with respect to x does not converge uniformly, it cannot be proven to satisfy the boundary conditions in Eq. (3).

The following technique is, therefore, employed. Take the limit of Eq. (A1) with respect to time:

$$\lim_{t\to\infty} T(x, t) = \frac{\rho_0 q_i}{k} \sum_{m=1}^{\infty} \frac{C(\lambda_m)\phi_m(x)\cos(\lambda_m c)}{\lambda_m^2} + \frac{\rho_0 q_i}{k} \frac{C(\lambda_0)\phi_0(x)\cos(\lambda_0 c)}{\lambda_0^2} [1 - \exp(-\kappa\lambda_0^2 t)] \quad \text{(A2)}$$

Then take the derivative of Eq. (A2) with respect to time

$$\frac{\partial T}{\partial t} = \frac{\rho_0 q_i \kappa C(\lambda_0)\phi_0(x)\cos(\lambda_0 c)}{k} [\exp(-\kappa\lambda_0^2 t)] \quad \text{(A3)}$$

Then solve Poisson's equation for this condition

$$\frac{\partial^2 T}{\partial x^2} = \frac{\rho_0 q_i C(\lambda_0)\phi_0(x)\cos(\lambda_0 c)}{k} [\exp(-\kappa\lambda_0^2 t)] \quad \text{(A4)}$$

The solution of this differential equation is

$$T(x, t) = \frac{\rho_0 q_i}{k\beta^2} C(\beta)\cosh[\beta(x - c)]\cosh(\beta c)\exp(\kappa\beta^2) + a_1 x + a_0 \quad \text{(A5)}$$

Where a_1 and a_0 are constants of integration. Enforcing the boundary conditions in Eq. (3) and equating the result to Eq. (A2) yields the following relation:

$$\frac{\rho_0 q_i}{k} \sum_{m=1}^{\infty} \frac{C(\lambda_m)\phi_m(x)\cos(\lambda_m c)}{\lambda_m^2} + \frac{\rho_0 q_i}{k} \frac{C(\lambda_0)\phi_0(x)\cos(\lambda_0 c)}{\lambda_0^2} = -\frac{\rho_0}{\alpha} \quad \text{(A6)}$$

From which it follows that

$$T(x, t) = -\frac{\rho_0}{\alpha} - \frac{\rho_0 q_i}{k} \sum_{m=1}^{\infty} \frac{C(\lambda_m)\phi_m(x)\cos(\lambda_m c)}{\lambda_m^2} \cdot \exp(-\kappa\lambda_m^2 t) + \frac{\rho_0 q_i}{k} \frac{C(\beta)\phi_0(x)\cosh(\beta c)}{\beta^2} \exp(\kappa\beta^2 t) \quad \text{(A7)}$$

Equation (A7) converges rapidly and $\partial T/\partial x$ converges uniformly on the interval $0 < x < c$.

References

[1]Wieting, T. J., and Shriempf, J. T., "Infrared Absorbtances of Partially Ordered Alloys at Elevated Temperatures," *Journal of Applied Physics*, Vol. 47, No. 9, 1976, pp. 4009–4011.

[2]Gallant, D. J., "Temperature Dependence of the Optical Absorption in Metals," Univ. of Southern California, Physics Thesis, Los Angeles, CA., June 1980.

[3]Hartman, P., *Ordinary Differential Equations*, 2nd ed., Birkhauser, Boston, MA, 1982, pp. 337–344.

[4]Ölcer, N. Y., "On the Theory of Conductive Heat Transfer in Finite Regions," *International Journal of Heat and Mass Transfer*, Vol. 7, 1964, pp. 307–314

Mixing of Multiple Coflowing Confined Laminar Streams

George C. Vradis* and M. Volkan Otugen†
Polytechnic University, Brooklyn, New York 11201

Introduction

THE improved design of chemical reactors, combustors, injectors, and other devices requiring the mixing of multiple streams, depends on our ability to obtain rapid and efficient diffusion of momentum, mass, and heat among these streams. In the traditional technology, the most frequently employed flow configuration for fluid mixing is the confined circular jet with or without a secondary coflowing stream. Recent requirements of improved performance, emphasizing robustness and efficiency, call for new approaches in the design of such rapid mixing equipment. In this note, it is proposed to study the possibility of using multiple streams to enhance the mixing process, thus resulting in more compact and less expensive devices.

The development of a circular jet with a coflow in a circular pipe has been studied for its significance in a number of engineering applications. The first systematic and comprehensive experimental study of the problem is that of Razinsky and Brighton.[1] In their work, pitot probes and hot-wire anemometry were used to study the effects of Reynolds number, velocity ratio (jet to secondary coflow velocity), and radius ratio (jet radius to pipe radius) on the flowfield. Other studies followed, including that of Suzuki et al.[2] which involved nonisothermal conditions, concentrating on different flow regimes. However, it was the study of Khodadadi and Vlachos[3] which provided a comprehensive set of measurements using the laser doppler anemometry (LDA) technique that led to a better understanding of the influence of large-scale organized structures on the flowfield, especially in the initial mixing region. In the same study a k-ε model of turbulence was employed to numerically predict the experimental data with limited success.

All studies up to now, however, involve the mixing of two coaxial streams (i.e., a central jet and a coflow around it). In the present work, the flow and heat transfer characteristics of systems with three coaxial laminar streams are numerically analyzed. The differences in the mixing process and the existence of separated flow regions resulting from the presence of the additional streams are determined. A second-order accurate, strongly implicit technique is employed for the solution of the governing fully elliptic Navier-Stokes equations. Results obtained for a range of the governing parameters are presented and demonstrate the increased mixing due to the presence of the third stream.

Governing Equations

The governing equations for the axisymmetric, steady, laminar, incompressible flow of a Newtonian fluid with constant properties in nondimensionalized form are

$$\nabla \cdot V = 0 \quad (1)$$

$$(DV/Dt) = -\nabla p + (1/Re)\nabla^2 V \quad (2)$$

$$(D\theta/Dt) = (1/Pe)\nabla^2\theta \quad (3)$$

Received Jan. 27, 1992; revision received June 10, 1992; accepted for publication June 24, 1992.

*Assistant Professor of Mechanical Engineering, Turbulent Fluid Mechanics Laboratory, Six Metro Tech Plaza. Member AIAA.

†Assistant Professor of Aerospace Engineering, Turbulent Fluid Mechanics Laboratory, Six Metro Tech Plaza. Member AIAA.

where $x = X/D_w$, $r = R/D_w$ are the nondimensionalized axial and radial distances with respect to the diameter D_w of the confining pipe, and $u = U/U_0$, $v = V/U_0$, $p = P/\rho U_0^2$, $\theta = (T - T_w)/(T_1 - T_w)$ are the corresponding nondimensionalized velocities, pressure, and temperature. U_0 is the bulk velocity of the incoming flow averaged over all streams, T_w is the temperature of the wall and T_1 is the temperature of the incoming stream along the axis of the pipe. The Reynolds number Re is based on U_0 and D_w. The Peclet number Pe is defined as the product of the Reynolds and Prandtl numbers.

Numerical Solution and Boundary Conditions

The numerical method employed in the present study for the solution of the governing fully elliptic equations has been used by the authors previously in solving various flow problems. Details on this method can be found in Vradis and Otugen.[4]

A 98 × 80 grid (in the axial and radial direction, respectively) was used, which was uniform in the radial direction ($\Delta r = 0.0125$) and variable in the axial direction, being fine at the inlet ($\Delta x = 0.02$) and increasing gradually towards the exit. The iterative procedure was terminated when the residual in the equations had reached a value of 10^{-5}. Grid refinement studies showed the results to be grid independent.

The flow geometry is shown as an insert in Fig. 3. The diameter of stream 1 (the central jet) is fixed equal to $0.1D_w$ in the present calculations. The width of stream 2, which divides stream 3 in two parts, is also kept fixed and equal to $0.1D_w$. The temperature and velocity profiles of all streams at the inlet are uniform. The nondimensional initial temperature of streams 1 and 2 is uniform and equal to $\theta_1 = \theta_2 = 1$, while the initial temperature of stream 3 and the uniform wall temperature are equal to $\theta_3 = \theta_w = 0$. The Prandtl number is constant throughout the calculations and equal to 0.7. The velocity ratio of the three streams is varied. Symmetry boundary conditions are employed along the pipe centerline. The downstream boundary is located far enough from the inlet for the fully developed flow conditions to be applicable. Since the required length of the computational domain for these conditions is not known a priori, after each computational run, the adequacy of the specified length was determined by checking if fully developed conditions are obtained at the exit.

Results and Discussion

For a Reynolds number of 100, the Nusselt number for the cases of one, two, and three coaxial streams are compared in Fig. 1. The Nusselt number, $Nu = hD_w/k$, is based on the bulk temperature T_b of the fluid along the cross section of the pipe, $\theta_b = (T_b - T_w)/(T_1 - T_w)$. In the case of one stream $U_2 = U_3 = 0$ and $\theta_2 = 0$, while in the case of two streams $U_2/U_1 = U_3/U_1 = 0.1$ and $\theta_2 = 0$. In the three streams case $U_2/U_1 = 1$ and $U_3/U_1 = 0.1$, and $\theta_2 = \theta_1 = 1$. In the case of the confined jet, the existence of the large recirculating zone at the inlet, 18 diam in length, results in a corresponding region of low Nusselt numbers. As the flow reattaches and becomes fully developed further downstream, the Nusselt number asymptotically tends towards its fully developed value of 3.66. In the two-stream case, where no separation occurs, the Nusselt number is initially very close to zero for a relatively small distance from the inlet due to the mixing layer between streams 1 and 2. Within this mixing layer, the temperature of stream 3 is almost equal to that of the wall, thus resulting in very small Nusselt numbers. In the three-stream case, the presence of a small recirculating region very close to the inlet, 3 diam in length, has a strong effect on the heat transfer rates. The recirculating bubble deflects the cold stream 3 strongly away from the wall, thus promoting its mixing with the warm stream 2. In addition, the recirculating flow carries the warm fluid to the wall and upstream towards the inlet. As a result, high-temperature gradients are established between wall and fluid, and thus, the Nusselt number rises extremely rapidly to a maximum at the reattachment point, followed by a gradual decline to the 3.66 value. A very substantial reduction in the size of both the hydrodynamic and thermal entrance regions is accomplished by introducing the third stream, through additional mixing layers and promotion of diffusion of momentum and heat.

The effect of the relative momentum of stream 2 on the heat transfer characteristics of the flow are demonstrated in Fig. 2 for $Re = 100$ and for $U_3/U_1 = 0.1$ and 0.5. In the first case, i.e., $U_3/U_1 = 0.1$, the higher shear rate obtained between streams 2 and 3, as the momentum of stream 2 is increased, results in the faster mixing of the two streams. The temperature close to the wall then increases faster and this results in increased heat transfer coefficients at the wall. If the momentum of stream 3 is increased to $U_3/U_1 = 0.5$, the tendency of the flow to separate is substantially decreased. The Nusselt numbers vary smoothly for the two smallest velocity ratios, which are lower than U_3/U_1, the heat exchange with the wall being determined by the wall boundary layer. As the velocity ratio of stream 2 exceeds that of stream 3, the developing shear layer between the two streams influences the heat exchange at the wall resulting in the local Nusselt number maxima in that region.

The effect of the position of stream 2 is shown in Fig. 3. The Nusselt number behavior in the entrance region is shown for $Re = 100$, $U_2/U_1 = 0.5$, $U_3/U_1 = 0.1$ and for four stream 2 locations. In the two smaller R_{2_i}/R_1 cases, adverse pressure gradients exist in the inlet region. In the two higher ratio cases, there are only favorable pressure gradients involved resulting in much higher Nusselt numbers.

The effects of the Reynolds number is shown in Fig. 4. An increase in the value of the Reynolds number does not necessarily imply an increase in Nusselt numbers as is the case

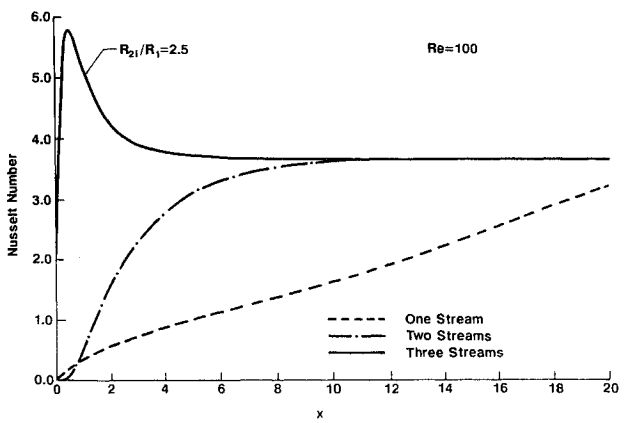

Fig. 1 Nusselt number for one, two, and three streams for $Re = 100$ and $R_{2_i}/R_1 = 2.5$.

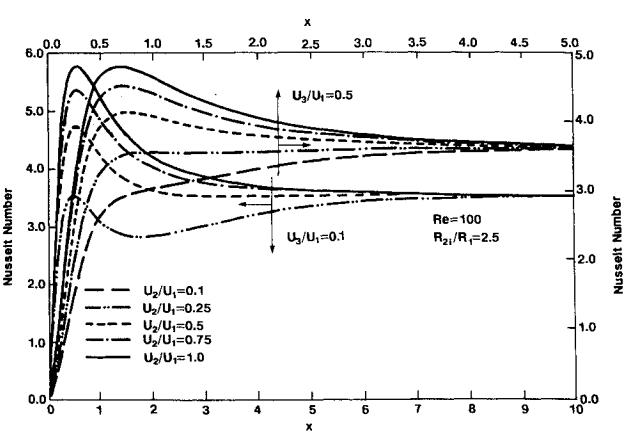

Fig. 2 Nusselt number for $Re = 100$, $U_3/U_1 = 0.1$ and 0.5, and $R_{2_i}/R_1 = 2.5$.

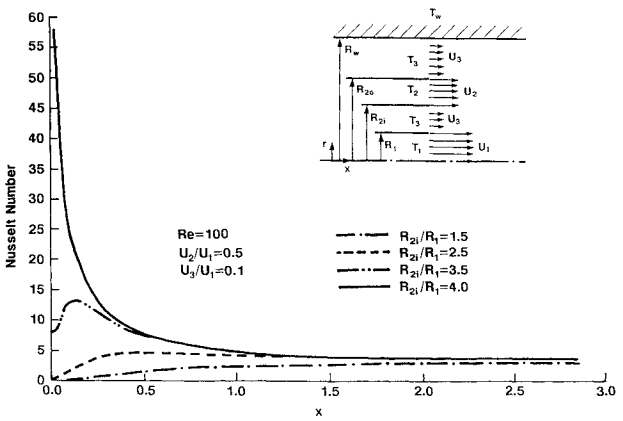

Fig. 3 Nusselt number for Re = 100, U_2/U_1 = 0.5 and U_3/U_1 = 0.1 and geometry.

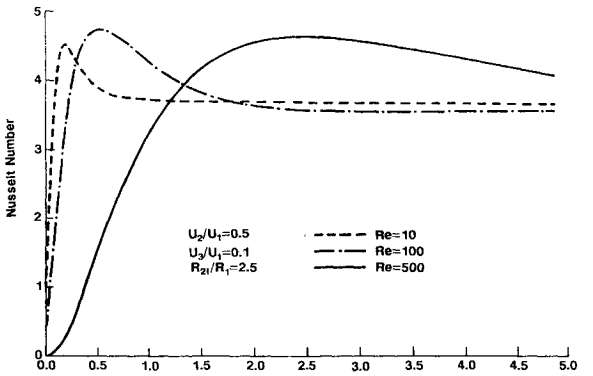

Fig. 4 Nusselt number for U_2/U_1 = 0.5 and U_3/U_1 = 0.1 and R_{2_i}/R_1 = 2.5.

in the Graetz problem. On one hand, an increase in the Reynolds number results in a decrease of the boundary-layer thickness along the wall, and a tendency for increased heat transfer rates. On the other hand, an increase in Reynolds number results in longer regions of very low favorable pressure gradients next to the wall. Such regions suppress the heat transfer process, therefore, resulting in lower Nusselt numbers. The combined result of these two opposing mechanisms is the behavior observed in Fig. 4.

In summary, the results demonstrate the fundamental differences between this flow and those of a simple confined jet, and of a confined jet in a single coflowing environment. Very substantial reductions in the entrance length are observed due to the addition of the third stream. Substantially higher Nusselt numbers are obtained in the three-stream case compared to the two- and single-stream cases. The distance of the intermediate stream from the pipe wall has a profound effect on the Nusselt number. The closer this stream is to the wall, the larger the Nusselt number becomes. In addition, the relative strength of the streams plays a major role in the thermal field. As the relative velocity of the middle coflowing stream is increased, the Nusselt number increases.

References

[1]Razinsky, E., and Brighton, J. A., "Confined Jet Mixing for Non-Separating Conditions," *Journal of Basic Engineering*, Vol. 93, Sept. 1971, pp. 333–349.

[2]Suzuki, K., Ida, S., and Sato, T., "Turbulence Measurements Related to Heat Transfer in an Axisymmetric Confined Jet and Laser Doppler Anemometer," *Proceedings of the 4th International Symposium on Turbulent Shear Flows*, Univ. of Karlsruhe, Karlsruhe, Germany, 1983, pp. 18.1–18.6.

[3]Khodadadi, J. M., and Vlachos, N. S., "Experimental and Numerical Study of Confined Coaxial Turbulent Jets," *AIAA Journal*, Vol. 27, No. 5, 1989, pp. 532–541.

[4]Vradis, G. C., and Otugen, M. V., "Laminar Mixing of Multiple Axisymmetric Confined Streams," 30th Aerospace Sciences Meeting, AIAA Paper 92-0369, Reno, NV, Jan. 6–9, 1992.

Analysis of Spectral Radiative Heat Transfer Using Discrete Exchange Factor Method

Yinqiu Zhang* and M. H. N. Naraghi†
Manhattan College, Riverdale, New York 10471

Introduction

IN the bandwise radiative heat transfer calculations, the absorption factor of some bands is large (resembling an optically thick medium), and in others it is small (resembling an optically thin medium). Furthermore, between bands the gas is transparent, making the problem one of radiative exchange between surfaces. Those methods that are capable of solving the radiative transfer problems for a wide range of optical thicknesses, as well as nonparticipating media, has the obvious advantage for analyzing such problems. When all surfaces are at the same temperature, or the gas contains soot or other gray components, the effect of the region between bands vanishes.

In this work we present a solution technique for this multiband problem using the discrete exchange factor (DEF) method. The versatility of the DEF method in solving spectral radiative transfer problems is demonstrated by presenting three example cases with different gas and surface conditions, including surfaces at different temperatures.

Analysis

In order to use the DEF method for analysis of spectral radiative transfer in an enclosure, the nongray distribution of radiative properties is subdivided into a finite number of wavebands. It is considered that the absorption coefficient is constant within each band and the medium is transparent outside the band. The gas properties are obtained using Edwards' wide band model.[1] The direct exchange factors are evaluated at each band using the formulations given in Refs. 2 and 3. In the regions between bands, where the gas is transparent, gas-to-gas and gas-to-surface exchange factors are zero, and only surface-to-surface exchange factors must be evaluated. The direct-spectral direct-exchange factors will then be used to calculate total exchange factors between nodal points at each band. Explicit matrix formulations presented in Ref. 2 can then be used to calculate spectral total exchange factors, i.e.,$(\overline{DS_iS_j})_v$, $(\overline{DS_iG_j})_v$, $(\overline{DG_iS_j})_v$, and $(\overline{DG_iG_j})_v$.

Once the spectral total exchange factors are determined, the heat fluxes and emissive powers of the surface and the gas nodes can be obtained at each band. The overall heat flux at node i is calculated by integrating the spectral heat flux distribution over all wave numbers v

$$q_i'' = \int_0^\infty q_{i,v}'' \, dv \tag{1}$$

This equation can be integrated numerically to yield the following discretized formulations for calculating the overall heat

Received June 25, 1992; revision received Sept. 27, 1992; accepted for publication Oct. 1, 1992.

*Graduate Student, Department of Mechanical Engineering.
†Associate Professor, Department of Mechanical Engineering.